applied sciences

MDPI

Article

Revisiting the Decomposition Process of Tetrahydrate Co(II) Acetate: A Sample's Journey through Temperature

Daniel Gutiérrez-Martín [1], Aurea Varela [1], José M. González-Calbet [1,2], Emilio Matesanz [3,*] and Marina Parras [1,*]

[1] Departamento de Química Inorgánica, Facultad de Ciencias Químicas, Universidad Complutense, 28040 Madrid, Spain; dangut04@ucm.es (D.G.-M.); aurea@ucm.es (A.V.); jgcalbet@ucm.es (J.M.G.-C.)
[2] ICTS ELECMI Centro Nacional de Microscopía Electrónica, Universidad Complutense de Madrid, 28040 Madrid, Spain
[3] Unidad de Difracción de Rayos X, Centro de Apoyo a la Investigación de Técnicas Químicas, Universidad Complutense, 28040 Madrid, Spain
* Correspondence: ematesanz@ucm.es (E.M.); mparras@ucm.es (M.P.)

Abstract: Cobalt oxides, CoO and Co_3O_4, were obtained from Co (II) acetate tetrahydrate. The thermal decomposition pathway of the starting product was followed by combining thermogravimetric analysis and in situ X-ray thermodiffraction. Under a nitrogen atmosphere, cobalt monoxide with Zn-blende and rocksalt polymorphs could be obtained almost as single phases at 330 and 400 °C, respectively. In addition to these oxides, a Co (II) oxyacetate, $Co_3O(CH_3COO)_4$, was stabilized as an intermediate phase. Under an air atmosphere, Co_3O_4 (spinel structure type) was obtained as the only final product. The involved phases in this thermal decomposition process were characterized with scanning and transmission electron microscopy (SEM and TEM, respectively).

Keywords: cobalt oxides; thermodiffraction; morphology; microstructure

Citation: Gutiérrez-Martín, D.; Varela, A.; González-Calbet, J.M.; Matesanz, E.; Parras, M. Revisiting the Decomposition Process of Tetrahydrate Co(II) Acetate: A Sample's Journey through Temperature. *Appl. Sci.* **2022**, *12*, 6786. https://doi.org/10.3390/app12136786

Academic Editors: Enrique Rodríguez-Castellón and María Luisa López

Received: 27 May 2022
Accepted: 29 June 2022
Published: 4 July 2022

1. Introduction

Transition metal oxides have several applications in different fields such as heterogeneous catalysis, magnetic data storage, energy storage, and battery materials. As a result, there has been growing interest in the development of new methods for the preparation of nanosized metal oxides with different sizes and shapes.

In particular, many articles have been devoted to the synthesis, microstructure, and properties of cobalt oxide nanoparticles due to their high potential as catalysts [1,2], gas sensors [3], and magnetic materials [4,5]. Cobalt oxides have been prepared by different procedures, e.g., the sol–gel process [6,7], hydrothermal synthesis [8], mechanochemical processing reactions [9], and combustion synthesis [10,11].

In bulk, cobalt oxide crystallizes in one of two stable phases, Co_3O_4 or rocksalt CoO. Co_3O_4 has a normal spinel structure [12] (SG. *Fd-3m*), with Z = 8, i.e., 8 unit formula (Co_3O_4) per unit cell. Oxygen ions are arranged in a cubic close-packed lattice (8 fcc unit cells) with Co (II) and Co (III) in the tetrahedral (1/8 occupation) and octahedral (1/2 occupation) sites, respectively. Rocksalt CoO is the stable phase of cobalt monoxide. In this polymorph, cobalt (II) ions are located in the octahedral sites of a cubic close-packed (fcc) arrangement of oxygen ions.

However, at the nanoscale, metastable CoO with wurtzite and sphalerite (Zn blende) structures can be stabilized [13]. In both, cobalt (II) is four-fold coordinated in a tetrahedral environment to oxygen ions that adopt a cubic close-packed lattice in the Zn blende (SG. *F-43m*) and a hexagonal arrangement in the wurtzite–CoO polymorph ($P6_3mc$). F. Huang et al. [14] stated that the formation of wurtzite ZnS is controlled by nucleation on the particle's surface and that the crystal growth of wurtzite is kinetically controlled by the radius of the sphalerite–wurtzite interface. R.W. Grimes et al. previously suggested that

wurtzite–CoO nucleates from zinc-blende crystallites, so the stabilized final phase depends on the Zn-blende particle size [15]. If the primary nuclei are small, the energy barrier for wurtzite formation can be overcome, thus enabling wurtzite formation. However, if said nuclei are large, the energy barrier is too high to allow for wurtzite formation, hence yielding Zn-blende CoO as the final product.

The growing interest in the physical properties of nanoparticles has driven the development of preparative methods. Among the different synthetic methods, the thermal decomposition of single-source precursors is a simple way to obtain metal oxides. Cobalt hydroxide [16], cobalt nitrate [17], cobalt carbonate [18], and cobalt oxyhydroxide [19] have proven to be effective solid precursors to obtain nanostructured Co_3O_4.

The three CoO polymorphs can also be obtained with the same synthetic procedure. The synthesis of CoO nanoparticles from Co (II) acetylacetonate as a single precursor in oleylamine was found to result in wurtzite and Zn-blende CoO [20]. Nanocrystals of wurtzite–CoO were isolated for the first time from the thermolytic decomposition of cobalt acetylacetonate in a high-temperature solvent (benzyl ether) [21]. By using the same precursor, I. Golosovsky et al. analyzed some of the parameters that determine the formation of wurtzite or Zn-blende polymorphs; they also performed a detailed magnetic characterization of both CoO nanoparticles [5,22].

In the early works on the synthesis of these oxides, all of them (Co_3O_4 and the three CoO polymorphs) were synthetized through the controlled thermal decomposition of cobalt (II) acetate tetrahydrate following the complementary use of diffraction and thermogravimetric techniques [15,23,24]. According to these results, this process goes through two main stages. At 150 °C, the dehydration of the starting acetate is complete, and a crystalline anhydrous acetate is stabilized at 200 °C. In the second step (275–310 °C), this new phase decomposes, giving rise to Zn-blende CoO, which transforms at 310 °C to a rocksalt polymorph. In any step of this process, wurtzite–CoO can be stabilized [24], although both polymorphs were present in samples prepared at 290 °C in argon [15]. In a later work, T. Wanjun et al., [25] described the formation of a basic cobalt acetate as an intermediate product in this thermal decomposition process.

In this work, we revisited the thermal decomposition process of $Co(CH_3COO)_2{\cdot}4H_2O$. The thermal decomposition of a precursor material has some advantages over other preparation methods including its simplicity, low cost, and ease of obtaining high-purity products. SEM and TEM were used to study the morphology and microstructure of the final oxides. In addition, we isolated the previously detected intermediate crystalline phase that corresponds to a Co(II) oxyacetate of chemical composition $Co_3O(CH_3COO)_4$.

2. Materials and Methods

Thermogravimetric analysis (TGA) was performed using a TG/DTA 6300 SII EXSTAR. About 15 mg of the sample were heated inside a Pt crucible at a constant rate of 2 °C/min from room temperature (RT) up to 400 °C before maintaining this temperature for 30 min. Afterwards, the sample was cooled down at 40 °C/min to room temperature. The experiments were carried out under N_2 and air atmospheres.

All the X-ray powder diffraction measurements (XRPD) were conducted with a Panalytical X'Pert PRO diffractometer with a copper tube and fast X'Celerator detector.

In situ non ambient X-ray diffraction experiments were carried on by using an Anton Paar HTK2000 high-temperature camera with platinum heating filament, and a secondary flat monochromator was used in the diffraction optics. For the temperature sweep under air, the camera was kept open. In the case of the experiments conducted under a nitrogen atmosphere, a continuous stream was running inside the camera throughout the experiment. For these experiments, the initial $Co(CH_3COO)_2{\cdot}4H_2O$ sample was gently ground with a mortar and pestle and then deposited as a thin layer of powder over the heating strip. The scans measured with this camera presented a broad band at $2\theta = 7^\circ$ corresponding to scattering coming out from the Kapton window of the camera cover.

Phase identification-oriented XRPD measurements were performed in reflection or transmission geometry depending on the sample appearance. In this case, samples were not ground, and they were mounted in a "zero background" silicon sample holder for the reflection measurements. For transmission XRPD scans, the sample was prepared in a 0.7 mm diameter borosilicate glass capillary.

The optics used for these reflection scans included a primary beam monochromator (Cu K alpha1 radiation). In the case of the capillary transmission measurements, the incident optics consisted of a focusing multilayer elliptical mirror (Cu K alpha radiation).

Phase identification analysis was conducted with Malvern Panalytical B.V. (Almelo, The Netherlands) X'Pert HighScore Plus v5.1.a software [26] to compare the scan peaks with ICCD PDF4+ database (2022 release) [27]. Identified phases are reported throughout the text with their PDF card numbers. The unit cell parameters of the intermediate cobalt oxyacetate phase were determined, with the reflections collected in a Bruker D8 Venture single crystal diffractometer (Cu radiation).

Samples for transmission electron microscopy (TEM) were ultrasonically dispersed in n-butanol and transferred to coated copper grids. Selected area electron diffraction (SAED) experiments and high-resolution transmission electron microscopy (HRTEM) were performed with a JEOL JEM 2100 electron microscope supplied with an Oxford INCA detector working at 200 kV.

The morphological study of the samples was carried out with a JEOL JSM 7600F scanning electron microscope using a graphite holder and a "gentle-beam" mode operating at an acceleration voltage of 15 kV.

3. Results

The decomposition process of commercial cobalt (II) acetate tetrahydrate, $Co(CH_3COO)_2{\cdot}4H_2O$ (*Aldrich* 208396 reagent grade), was followed by combining thermogravimetric analysis (TGA) and in situ X-ray thermodiffraction.

3.1. Thermal Decomposition under Nitrogen Atmosphere

Figure 1a shows the XRD pattern of the commercial starting material. The whole pattern corresponds to $Co(CH_3COO)_2{\cdot}4H_2O$ (PDF 00-025-0372), although a small intensity extra peak can be appreciated at $2\theta = 10.3°$. This could correspond to the most intense reflection (hkl) of the Co (II) acetate dihydrate that may have been present in the commercial product in a low ratio. The intensity of this reflection seemed to increase after the sample grinding process (Figure 1b).

Figure 2 shows the TG curve for cobalt (II) acetate tetrahydrate under an N_2 atmosphere. Under the experimental conditions described in the previous section, the decomposition process of the $Co(CH_3COO)_2{\cdot}4H_2O$ starting material took place through three stages labeled as A, B, and C in the figure.

To identify the intermediate products formed during this process, an in situ thermodiffraction study was performed. This experiment consisted of a temperature sweep under N_2 every 10 °C from room temperature up to 400 °C and then down to 270 °C. Temperature ramps of 10 °C/min were used for increasing or decreasing the temperature between steps, and the temperature was kept constant during the X-ray diffraction scans. Figure 3 shows a 2D contour plot depicting the thermal evolution of the X-ray diffraction (XRD) maxima of the different products involved in this decomposition process. This type of plot enables one to easily observe the decomposition of a phase or the emergence of a new one and thus select the most suitable temperatures to collect X-ray data throughout the decomposition process.

The experimental weight loss of the first step (from RT up to 110 °C), $\Delta W = 30.4\%$, was close to that corresponding to the total dehydration of the starting sample ($-4\ H_2O$/mol: $\Delta W = 28.9\%$). The slight slope change observed at 75 °C could indicate a different rate in the release of water molecules. According to Figure 3, the starting $Co(CH_3COO)_2{\cdot}4H_2O$ stayed up to 70 °C, when its characteristic XRD lines were no longer visible. Note that

the line corresponding to the most intense reflection of $Co(CH_3COO)_2{\cdot}2H_2O$ ($2\theta \approx 10°$) remains visible after the full transformation of the tetrahydrate form (70 °C scan), and its intensity even slightly increases. By the 80 °C scan, as the water was lost, the diffraction maxima intensity of the hydrated acetates decreased and no crystalline phase emerged, although a broad maximum can be observed at $2\theta \approx 9°$. These features are better observed in the XRD patterns collected at RT, 60, 70, and 90 °C (Figure 4a–d). As can be seen in the TGA plot, the dehydration process was completed at 110 °C and the weight remained almost constant up to 200 °C.

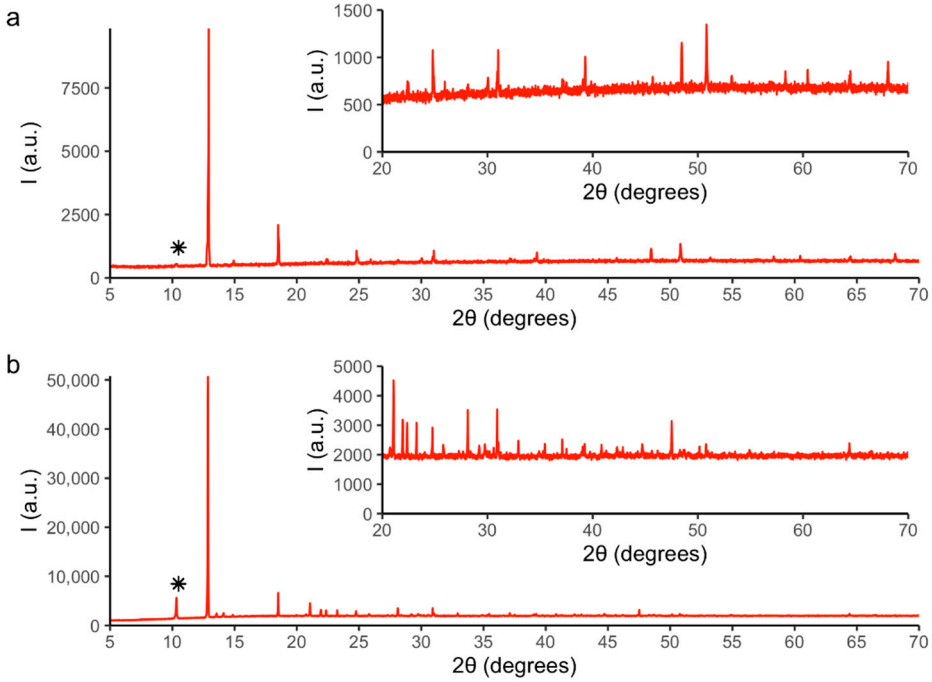

Figure 1. X-ray powder diffractograms of commercial cobalt acetate tetrahydrate before (**a**) and (**b**) after grinding. The most intense reflection of the dihydrated cobalt acetate (marked with an asterisk in the figures) is visible in both diagrams, although its intensity is clearly increased in the ground sample. An enlargement of both diffraction patterns is shown at the inset.

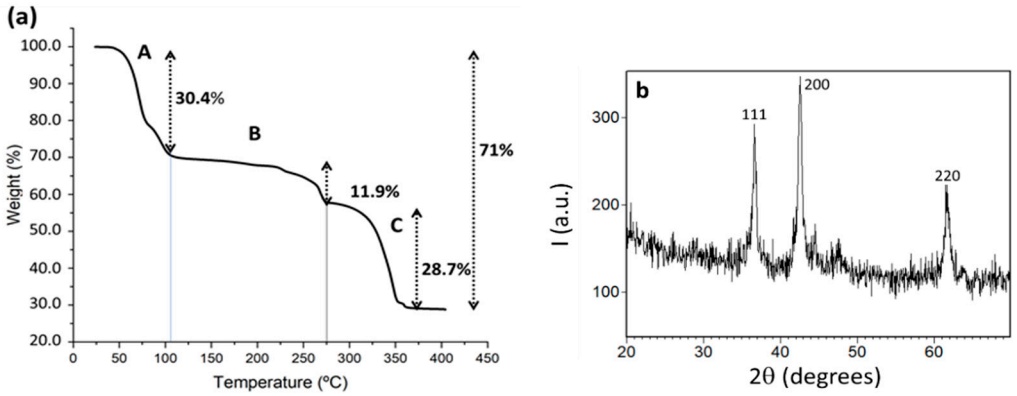

Figure 2. (**a**) TGA plot of the decomposition of commercial $Co(CH_3COO)_2{\cdot}4H_2O$ under N_2 atmosphere. Step **A**: from RT up to 110 °C; Step **B**: from 110 to 275 °C; Step **C**: from 275 to 400 °C. (**b**) XRD pattern of the final product of the TGA analysis. All the intense maxima correspond to the CoO rocksalt (PDF 00-048-1719).

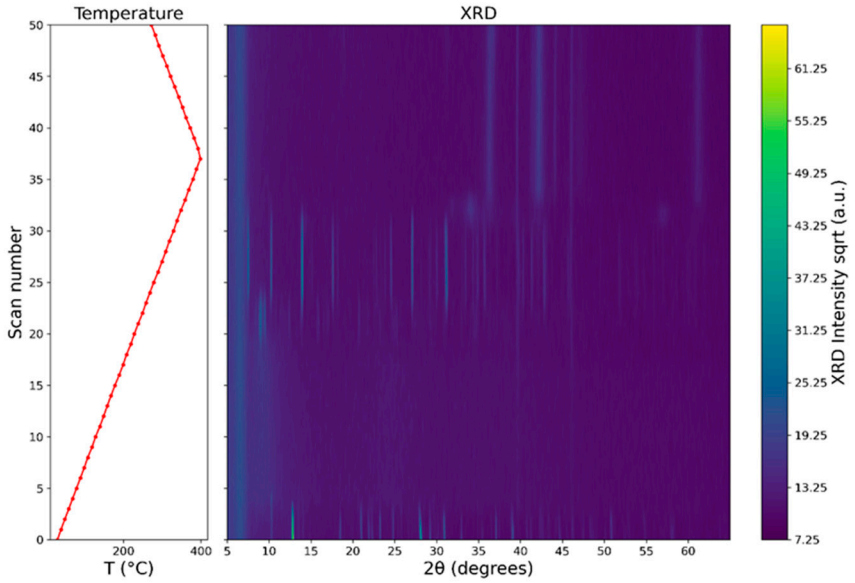

Figure 3. X-ray powder diffraction thermal evolution for cobalt (II) acetate tetrahydrate under N_2 between RT and 400 °C (heating) and then cooled down to 270 °C. Intensity scale as square root. *Note the presence of a width scattering bump around 2θ = 7° coming out from the camera, as well as main platinum peaks around 41.0° and 47.7°. 2θ values (ICDD PDF card 01-087-0642) produced by the camera heating element are present in some scans.*

It is not easy to determine which intermediate compounds were formed in this temperature range. After searching through the Cambridge Structural Database [28], several cobalt acetate structures with different water content were found. Between the starting $Co(CH_3COO)_2{\cdot}4H_2O$ (CSD-1491979 [29] and CSD-225647 [30]) and the anhydrous $Co(CH_3COO)_2$ (CSD-715832 [31]), two intermediate crystalline phases—$Co(CH_3COO)_2{\cdot}2H_2O$ (CSD-138992 [32] and CSD-715831 [31]) and $[Co(CH_3COO)_2]_5.H_2O$ (CSD-1127997 [33])—have been described. Thus, from a chemical point of view, it would be reasonable to think that this could be the path of dehydration, but none of these phases were detected by XRD (although we were able to stabilize the dihydrate, crystalline $Co(CH_3COO)_2{\cdot}2H_2O$ under the experimental conditions described in Section I of Supporting Information). In addition, the hydration water could hydrolyze the acetates and both processes could occur simultaneously, giving rise to the formation of basic acetates. In this sense, intermediate phases of general formula $Co(OH)_x(CH_3COO)_{2-x}$ or $CoO_x(CH_3COO)_{2-2x}$ could also be present as non-crystalline compounds, since none were detected by X-ray diffraction.

From 200 to 275 °C, the sample quickly lost weight until a total ΔW of ~11.95%, indicating the partial decomposition of acetate groups. No significant change in the intensity of the diffraction lines (see Figure 3) up to a temperature close to 220 °C was observed; from this, the sample crystallinity increased, as evidenced by the presence of two well-defined lines at around 2θ ≈ 9–9.5°. Finally, around 250 °C, a new crystalline phase appeared. Figure 5a–d shows the obtained XRD patterns for some selected temperatures in the 200–280 °C range. At 200 °C (Figure 5a), only a broad diffraction maximum centered at 2θ ≈ 9–9.5 ° can be observed; this splits in two well-defined reflections at a temperature close to 230 °C, with a significant increase in the sample crystallinity (Figure 5b). At this stage of the decomposition process, following the previous dehydration step, it has been suggested that the formation of $Co(OH)_x(CH_3COO)_{2-x}$ or/and $CoO_x(CH_3COO)_{2-2x}$ [24] occurs as intermediate phases that, according to our experimental data (ΔW of ~11.95%), should correspond to $Co_2(OH)(CH_3COO)_3$ and $Co_5O(CH_3COO)_8$. However, there are no data to support the possible stabilization of any of these phases, so the crystalline product emerging at 230 °C remains an unidentified phase (or phases).

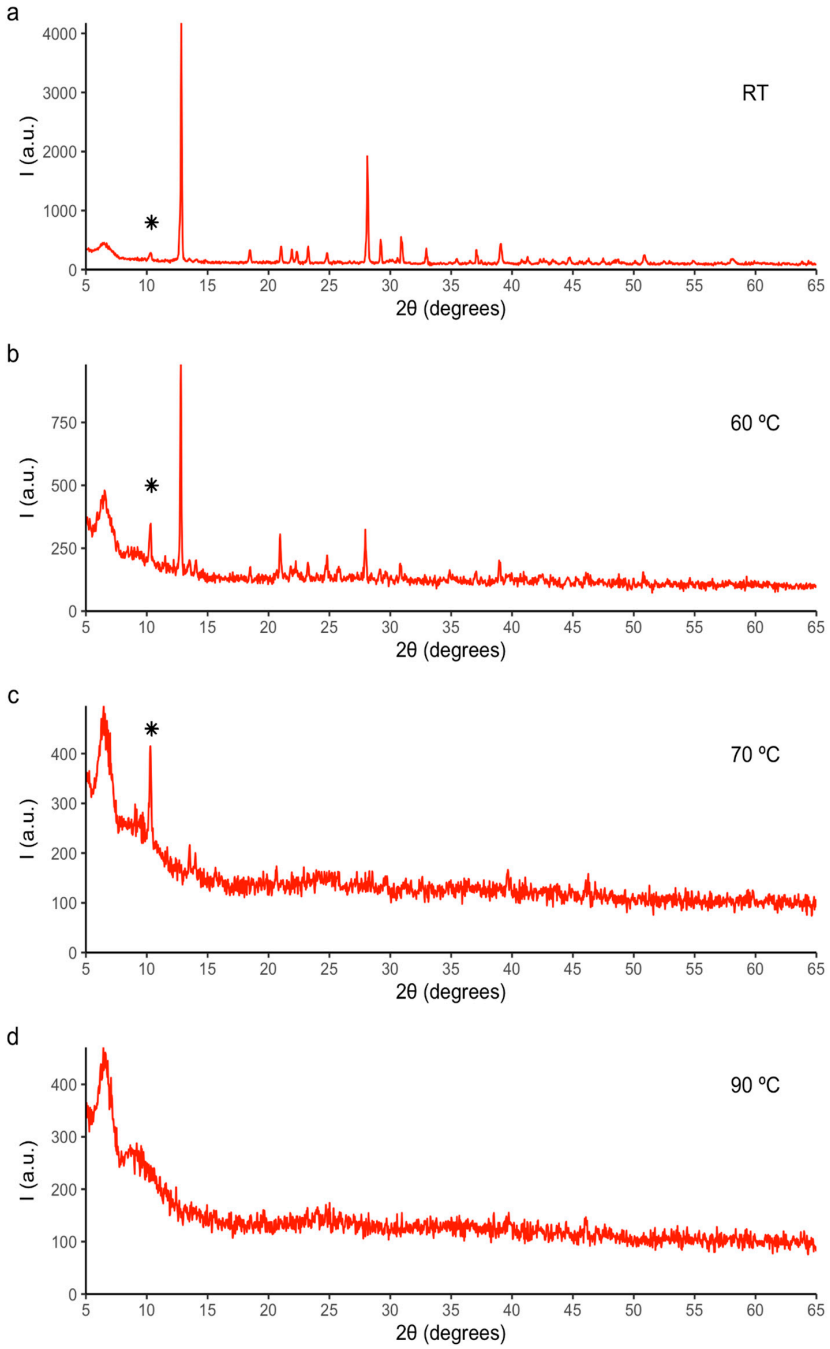

Figure 4. X-ray powder diffraction of cobalt (II) acetate commercial sample heated under N_2 atmosphere at: (**a**) room temperature, (**b**) 60 °C, (**c**) 70 °C, and (**d**) 90 °C. Main phase in the starting room temperature scan is the cobalt acetate tetrahydrate (PDF-00-025-0372), but the dihydrate phase (PDF-00-022-1080) can also be observed as a minor phase (main peak marked with an asterisk in (**a**–**c**) scans).

From 250 to 280 °C, the intensity of these maxima decreased, and the new emerging phase (Figure 5c) became the only crystalline one (Figure 5d). In previous works, this phase has been associated with the formation of different stable intermediate compounds. Wanjun et al., [25] suggested that this intermediate product corresponds to $Co(OH)_{0.8}(CH_3COO)_{1.2}$, whereas Grimes et al. [24] identified it as an acetate oxide of composition $Co_4O(CH_3COO)_6$. However, our results indicate that the new phase did not correspond to either one of these. In fact, as shown in Figure 5d, the whole XRD pattern at 280 °C perfectly matches that of PDF 00-022-0595 (observed quality) corresponding to a

cobalt (II) oxyacetate, $C_8H_{12}Co_3O_9$ (i.e., $Co_3O(CH_3COO)_4$) reported by J.L. Doremieux [34]. The experimental weight loss from anhydrous cobalt acetate (close to 18%) was consistent with the formation of this phase (19.2%). As described below, we were able to isolate this new phase.

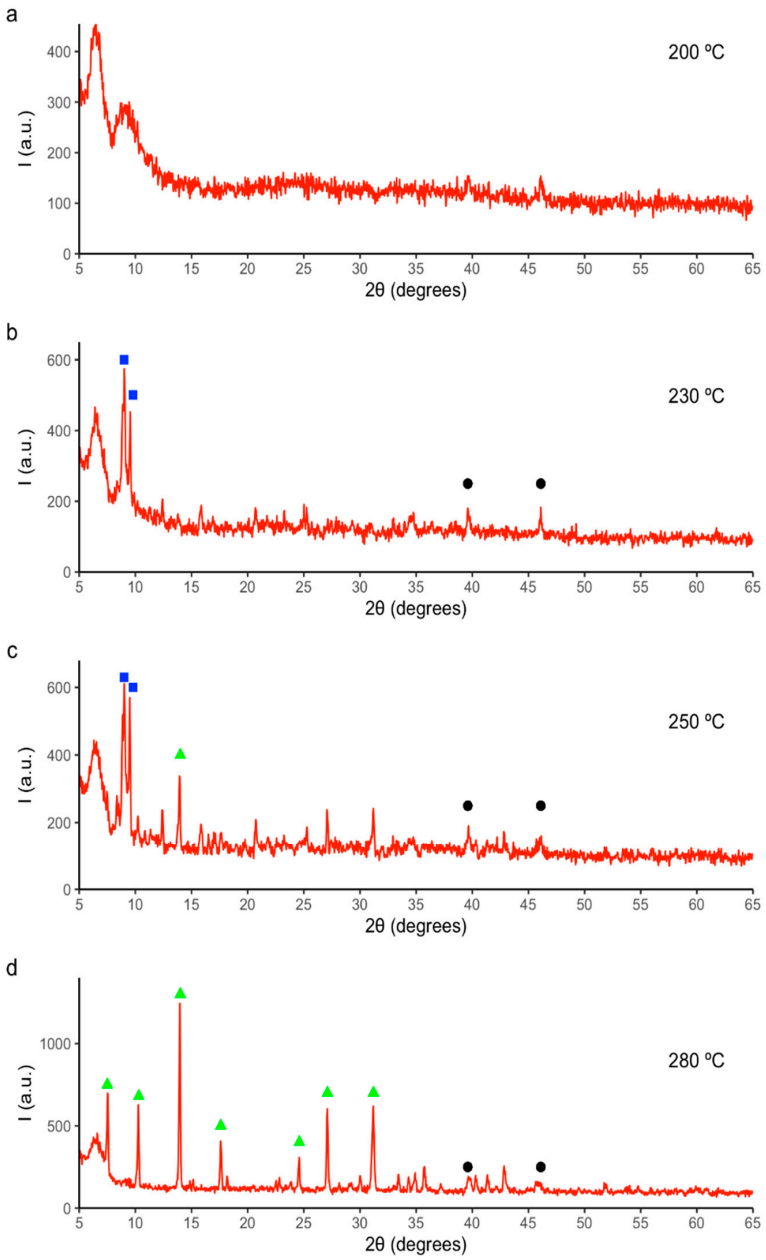

Figure 5. X-ray powder diffraction of cobalt acetate tetrahydrate commercial sample heated under N_2 atmosphere at (**a**) 200 °C, (**b**) 230 °C, (**c**) 250 °C, and (**d**) 280 °C. Main peaks of present phases are marked as follows: black circle for platinum (PDF-01-087-0642), green triangle for cobalt oxide acetate (PDF-00-022-0595), and blue square for an unknown phase.

From 275 °C (stage C in the TG curve), the sample continuously lost weight up to 370 °C; this mass remained constant during the cooling process until room temperature. As can be seen in Figure 3, from 340 °C, a new set of lines appears in the 2θ ≈ 32–37° range. Above 350 °C, the observed lines correspond to a mixture of CoO Zn-blende, wurtzite, and rocksalt polymorphs [13]. These structural changes can be better observed in Figure 6a–c. At 340 °C, the appearance of extra broad diffraction maxima (in the 2θ ≈ 32–37° range)

evidences the beginning of the abovementioned acetate oxide decomposition. At 360 °C, the most intense reflections correspond to cubic CoO Zn-blende, wurtzite, and rocksalt polymorphs (Figure 6b). Increasing the temperature further stabilized the rocksalt polymorph, which was the main phase at 400 °C, and a small fraction of hexagonal cobalt metal was also visible as minority phase (Figure 6c). Accordingly, from the starting $Co(CH_3COO)_2{\cdot}4H_2O$ phase, the total weight loss (ΔW = 71%) nicely matched the stabilization of a cobalt (II) monoxide, CoO, as major final product (see Figure 2b).

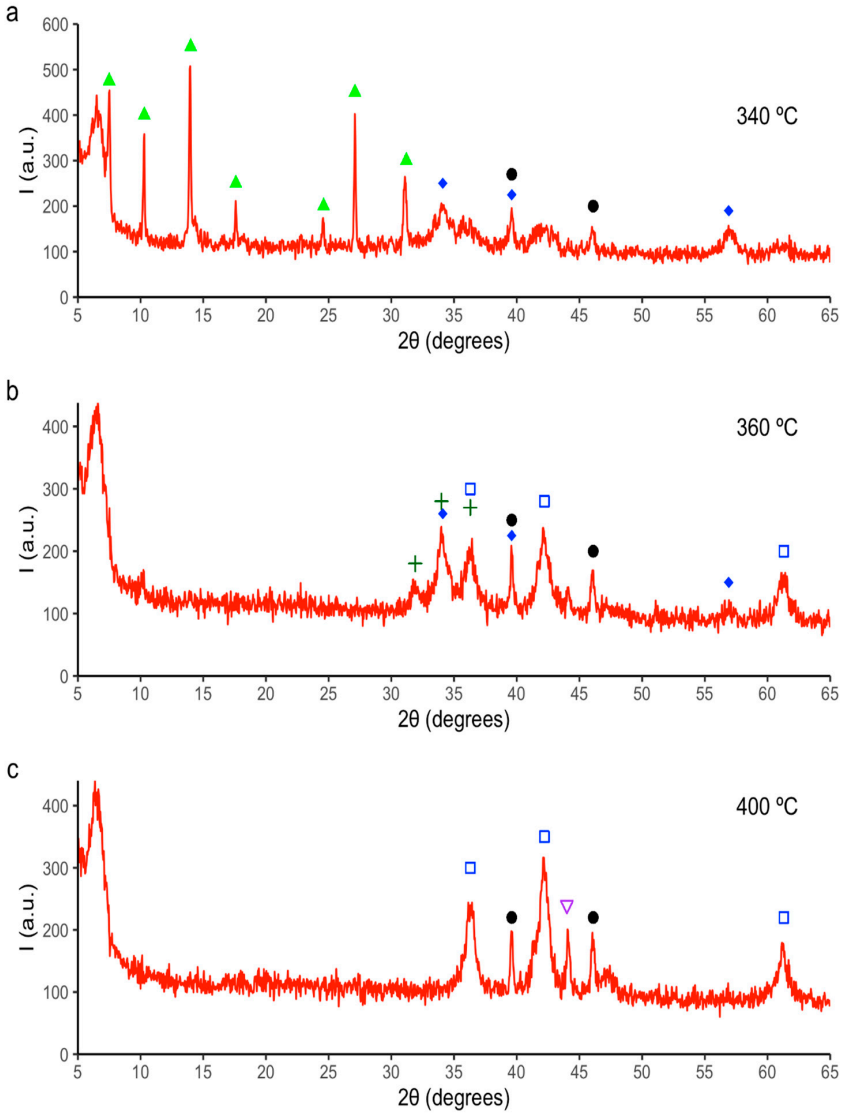

Figure 6. X-ray powder diffraction of cobalt (II) acetate tetrahydrate commercial sample heated under N_2 atmosphere at (**a**) 340 °C, (**b**) 360 °C, and (**c**) 400 °C. Main peaks of identified phases are marked as follows: black circle for platinum (PDF-01-087-0642), green triangle for cobalt oxide acetate (PDF-00-022-0595), blue diamond for CoO Zn-Blende (PDF-00-042-1300), dark green cross for CoO Wurtzite (PDF-04-005-4913), blue square for CoO rocksalt (PDF 00-048-1719), and purple inverted triangle for Co (PDF-01-089-4308).

A scheme showing the stabilized phases in the different stages of this thermal decomposition process is included in Supporting Information as Scheme S1.

3.2. Intermediate Phases

To isolate the different intermediate phases described above, a commercial $Co(CH_3COO)_2{\cdot}4H_2O$ sample was heated to selected temperatures in the high-temperature

XRD chamber to monitor the in situ formation of the desired product. From each temperature, the sample was quenched to RT. Below, we discuss the obtained results.

3.2.1. $Co_3O(CH_3COO)_4$ Oxyacetate

To stabilize the cobalt oxyacetate, the commercial cobalt acetate sample was heated in the high-temperature diffractometer chamber under N_2 while monitoring the thermal evolution. At 310 °C, the transformation to the target compound (PDF-00-022-0595) $Co_3O(CH_3COO)_4$ was complete. After cooling down the sample, a number of pink crystallites were collected for further characterization.

Measuring one selected crystal by X-ray single crystal diffraction allowed us to determine the unit cell of the compound. The cell parameters of the resulting orthorhombic cell were a = 6.5314(6) Å, b = 9.2502(17) Å, and c = 23.102(4) Å, with *Imma* as a possible space group. This unit cell was checked against the obtained powder diffraction pattern and showed a good agreement (Figure S2 of the Supporting Information).

3.2.2. Zn-Blende–CoO Polymorph

Following the previous results, a fresh commercial $Co(CH_3COO)_2{\cdot}4H_2O$ sample was heated in the X-ray chamber up to 332 °C under a nitrogen atmosphere. At this temperature, CoO with Zn-blende structure seemed to be stabilized as single phase (the 2D plot depicted in Figure 7a shows the thermal evolution of the sample). From 332 °C, the sample was quenched to RT. The XRD pattern of the obtained green product, shown in Figure 7b, matches that of PDF-00-042-1300, which corresponds to the cubic CoO.

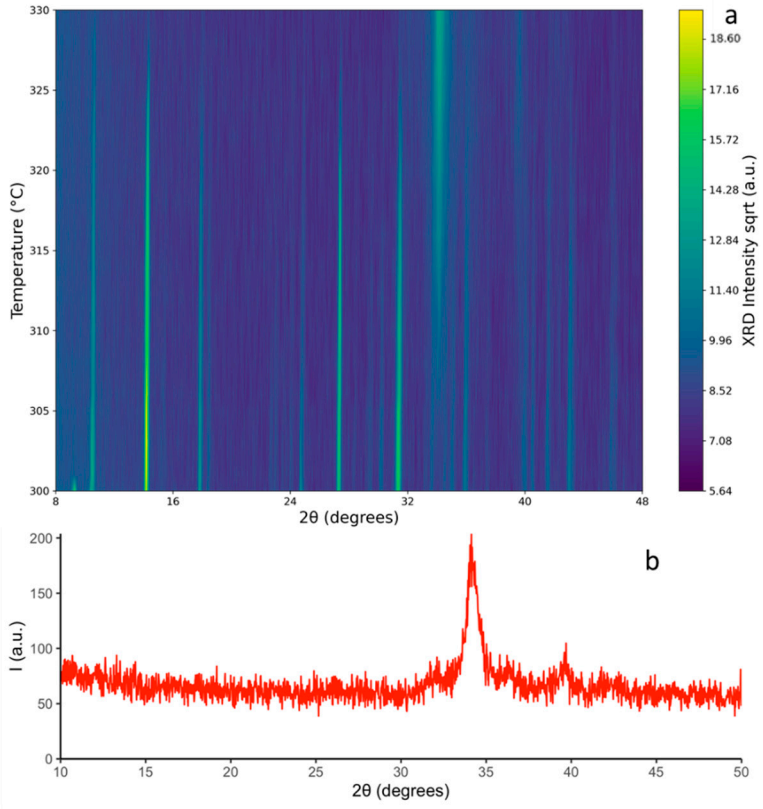

Figure 7. (**a**) X-ray powder diffraction thermal evolution of commercial cobalt (II) acetate heated under N_2 atmosphere from 300 to 332 °C in 2 °C steps. The experiment was stopped as soon as only Zn-blende-type structure for CoO was observed; (**b**) XRD pattern of the final product obtained at 332 °C, showing the two characteristics peaks of Zn-blende-type CoO (PDF-00-042-1300).

Under the experimental conditions described above, the wurtzite polymorph was not stabilized. As we mentioned in the introduction, a wurtzite polymorph nucleates from Zn-blende and the size of the formed primary nuclei strongly influences the growth of the wurtzite polymorph [13,23]. If these nuclei are larger, the obtained final phase is the Zn-blende; if they are small, however, the wurtzite polymorph can be stabilized [14,15]. Pure wurtzite CoO has been obtained from the thermal decomposition of cobalt acetylacetonate in refluxing benzyl ether [21]. Moreover, I.V. Golosovsky et al., [22] studied the main parameters determining the growth of either hexagonal or cubic polymorphs (solvents or surfactants, heating rate, reflux temperature or time . . .). According to the thermal decomposition of the acetate, the nucleus of Zn-blende CoO must have been large enough to prevent its transformation into the wurtzite polymorph that was never obtained as a single phase. The Zn-blende/wurtzite ratio was strongly dependent on the conditions in which the experience was carried out (see Section III.3. in Supporting Information).

3.2.3. Rocksalt CoO Polymorph

This polymorph was the main phase at temperatures above 350 °C and appeared as a single phase at around 400 °C. Therefore, a sample of $Co(CH_3COO)_2 \cdot 4H_2O$ was heated in the X-ray chamber up to 400 °C under a nitrogen atmosphere and quenched to RT. Figure 8 shows the XRD pattern of the obtained product. The diffraction maxima of rocksalt CoO (PDF-00-048-1719) can be identified, and three more peaks that should correspond to metallic cobalt (PDF-01-089-4308) are also visible.

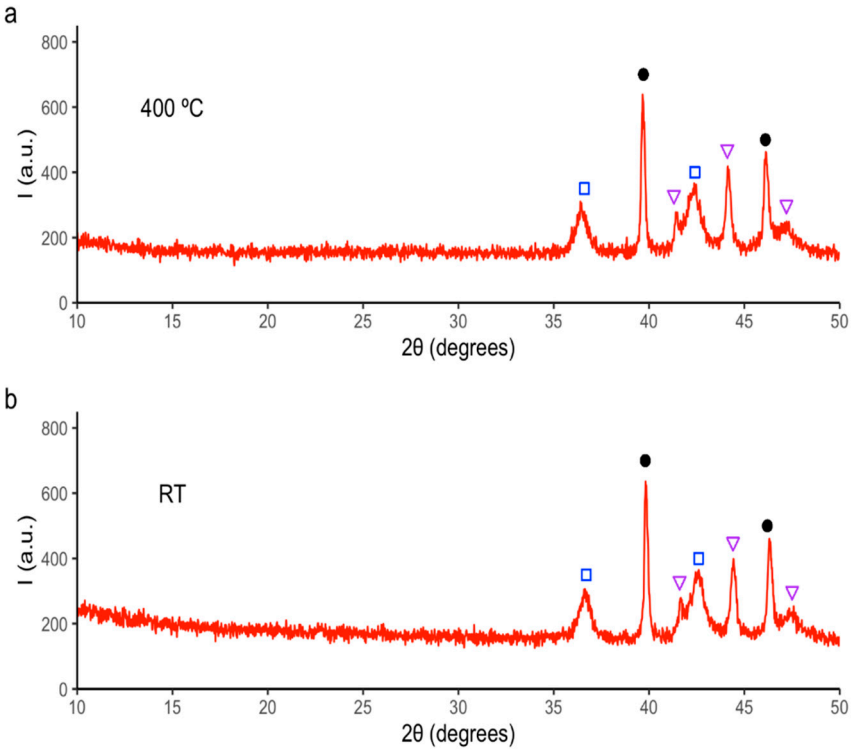

Figure 8. X-ray powder diffraction of cobalt acetate tetrahydrate heated under N_2 atmosphere at 400 °C (**a**) and quenched back to 25 °C (**b**). Main peaks of identified phases are marked as follows: black circle for platinum (PDF-01-087-0642), blue square for CoO rocksalt polymorph (PDF 00-048-1719), purple inverted triangle for Co (PDF-01-089-4308), and orange crossed circles for Co_3O_4 (PDF-01-086-8289).

The presence of cobalt particles in the sample could have been due to the CoO reduction; however, under the working conditions, it seems most plausible that a charge disproportionation process occurred ($4CoO \rightarrow Co_3O_4 + Co$). In a new experiment, the same commercial cobalt acetate sample was heated at 400 °C under N_2, and X-ray diffraction data were repeatedly collected in short scans (approximately 8 min long). In the first XRD scan (Figure 9a), only metallic Co and rocksalt CoO polymorph were detected; however, the last pattern (collected after 27 min while keeping the sample at 400 °C) (Figure 9) demonstrated the emergence of Co_3O_4 while the intensity of the reflection associated with metallic Co remained constant. According to this result, we think that the Co_3O_4 resulting from the CoO disproportionation was almost amorphous and therefore not detected by X-ray diffraction. The crystallinity of the formed Co_3O_4 increased with time, becoming clearly visible by XRD after about 30 min at 400 °C.

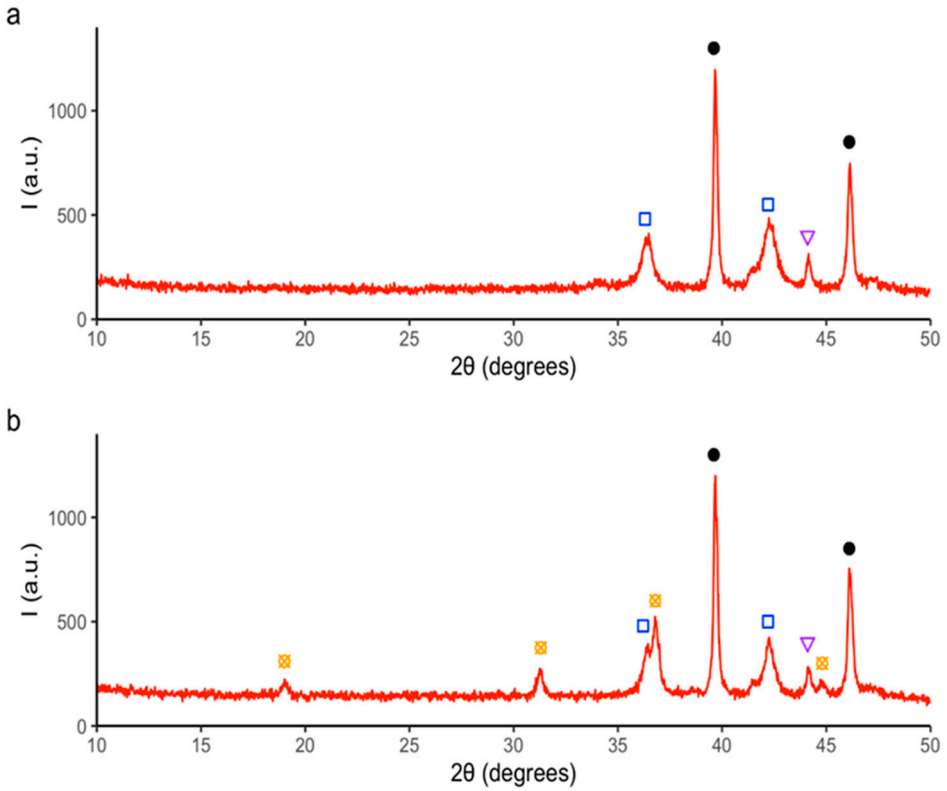

Figure 9. X-ray powder diffraction of cobalt acetate tetrahydrate heated under N_2 atmosphere at 400 °C. The sample was kept at 400 °C while several scans were measured. Starting time difference between the first (**a**) and the last one (**b**) was 27 min. Main peaks of identified phases are marked as follows: black circle for platinum (PDF-01-087-0642), blue square for CoO rocksalt polymorph (PDF 00-048-1719), purple inverted triangle for Co (PDF-01-089-4308), and orange crossed circle for Co_3O_4 (PDF-01-086-8289).

3.3. Morphological and Microstructural Characterization

We used scanning electron microscopy (SEM) and transmission electron microscopy (TEM) to characterize the morphological and microstructural features of our samples (detailed study is described in Section III of the Supporting Information). Below, we describe the most relevant results.

Figure 10b shows the morphology of the new cobalt (II) oxyacetate $Co_3O(CH_3COO)_4$ phase described above (fuchsia-pink color). In most of the particles, the elongated plate-like morphology of the starting acetate $Co(CH_3COO)_2 \cdot 4H_2O$ (Figure 10a) was retained, although the particle size was smaller at close to 3–30 μm in length. In addition, aggregates

of variable size, formed by round-shaped nanoparticles, were also observed (Figures S3 and S4 in Supporting Information).

The SEM images of the green Zn-blende CoO polymorph (obtained by quenching at 332 °C/N_2) show the presence of bundles of chains and sheets formed by nanoparticles of rounded (spherical) shape with a homogeneous particle size distribution within the nanometric scale (average size of 100 nm). These nanoparticles joined each other, forming micrometric planes and chains of variable length (Figure S8 in SI).

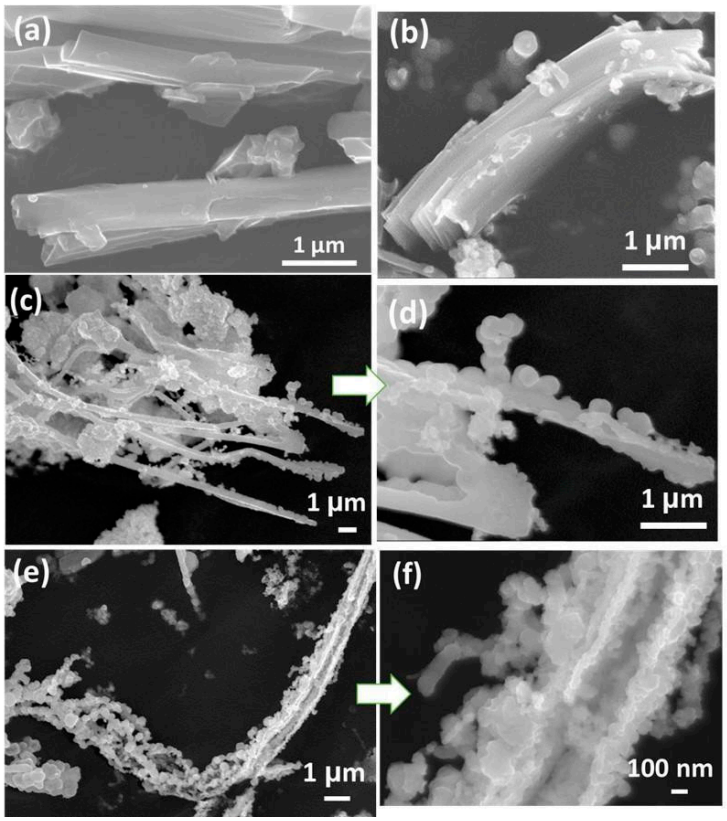

Figure 10. SEM micrographs of: (**a**) lightly ground commercial cobalt (II) acetate tetrahydrate sample, (**b**) elongated plates microcrystals of Co(II) oxyacetate $Co_3O(CH_3COO)_4$, (**c**) cubic blende CoO polymorph at low magnification 7000× and (**d**) enlargement of (**c**), and (**e**) rocksalt CoO polymorph at (7500×) and (**f**) at high-magnification (50,000×).

This polymorph retained the morphological features of $Co_3O(CH_3COO)_4$, indicating a certain topotactic relationship between them. After the decomposition process, its plate-like morphology was maintained in the cobalt oxide. This morphology was formed by highly homogeneous nanoparticles maintaining the particle packing of the precursor and leading to a sheet-assembling morphology (Figure 10c,d).

Finally, the morphological study of the rocksalt CoO polymorph (Figure 10e,f) revealed quite homogeneous particles with rounded shapes and sizes on the nanometric scale (close to 100 nm).

Figure 11 corresponds to the TEM images of the CoO Zn-blende type. All the particles showed a spherical morphology and an average size between 5 and 10 nm (Figure 11a). Figure 11b shows the corresponding FFT pattern characteristic of a polycrystalline sample that can be indexed to the Zn-blende structure, where the distances of 0.270 and 0.24 nm correspond to 111 and 002 interplanar distances, respectively. Figure 11c,d shows the HREM images and their corresponding FFT of one nanocrystal of the sample along the [001] projection. The distances of 0.24 nm correspond to the (200) crystal planes of the cubic Zn-blende structure.

The TEM image of rocksalt CoO shown in Figure 12 shows agglomerates of crystalline faceted nanoparticles with sizes on the nanometer scale (between 5 and 10 nm in length). The corresponding FFT pattern, characteristic of a polycrystalline sample, is shown in the Figure 12b. The strong ring patterns can be well-indexed to the fcc CoO structure, where the distances of 0.243 and 0.211 nm correspond to 111 and 002 interplanar distances, respectively, of rocksalt-CoO oxide.

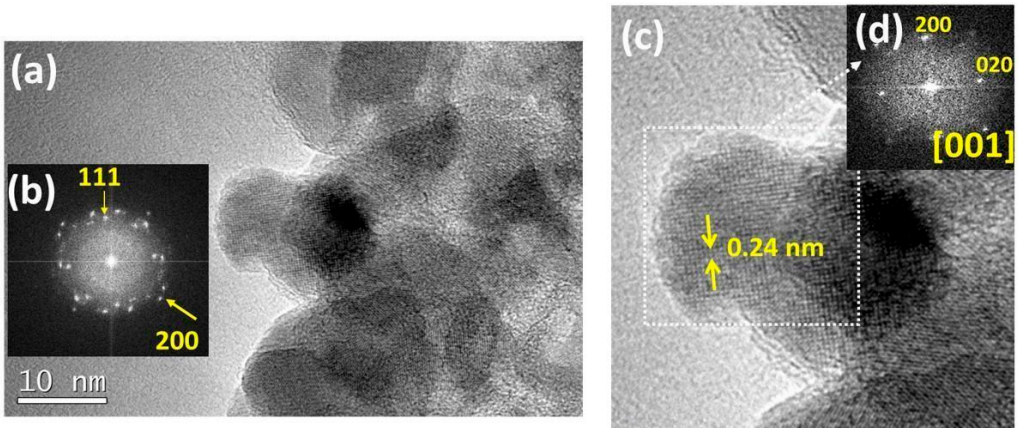

Figure 11. (**a**) TEM image of Zn-blende CoO nanoparticles and (**b**) corresponding fast Fourier transform (FFT) pattern. (**c**) HRTEM images and (**d**) corresponding FFT pattern of a representative nanocrystal along [001] zone axis.

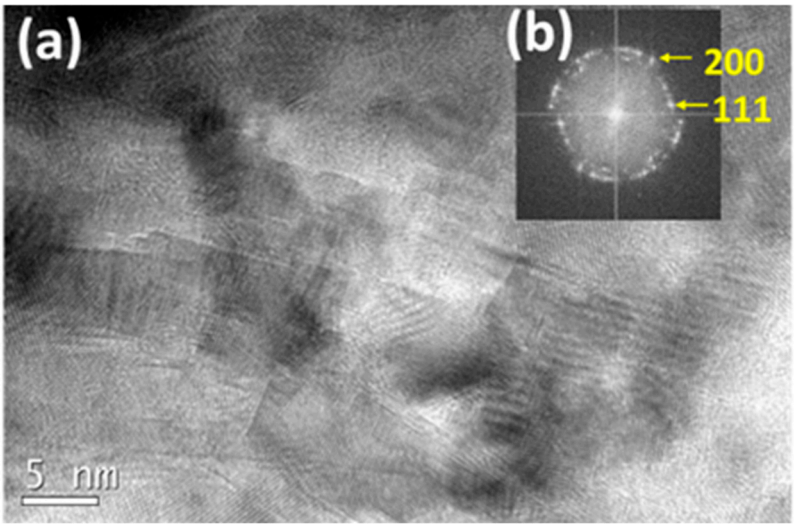

Figure 12. (**a**) TEM image of rocksalt-CoO nanoparticles and (**b**) corresponding fast Fourier transform (FFT) pattern.

3.4. Thermal Decomposition under Air Atmosphere

Figure 13a shows the result of TG analysis in air for Cobalt (II) acetate tetrahydrate. The first decomposition step (Δw = 30%)) was analogous to that obtained in a nitrogen atmosphere and corresponded to the total dehydration of the sample. Above 175 °C, the acetate groups began to decompose in such a way that at 270 °C, the exothermic decomposition abruptly ended. The total weight loss nicely agreed with the formation of the Co_3O_4 oxide. Actually, the XRD pattern of the ATG final product, shown in Figure 13b, perfectly matched that of PDF-00-086-8289, corresponding to the Co_3O_4 spinel.

A 2D contour plot of the thermal evolution of the X-ray diffraction (XRD) maxima intensity of the total decomposition process is shown in Figure S9 in Supporting Information. Figure 14a–h depicts the XRD patterns at some selected temperatures. As in the results obtained in N_2, the sample became amorphous when the hydration water was lost. The cobalt acetate tetrahydrate stayed up to 70 °C; from this temperature onwards, only the dihydrate acetate (present in the commercial product as impurity phase) remained up to around 100 °C (Figure 14a–d). No crystalline phase was observed in the 100–200 °C temperature range (Figure 14d,e). The 270 °C scan (Figure 14f) signifies the presence of Co_3O_4 as the only crystalline phase. From this temperature and up to 400 °C (Figure 14g), no structural change could be observed other than an increase in the crystallinity of the sample. This phase was maintained during cooling until room temperature (Figure 14h).

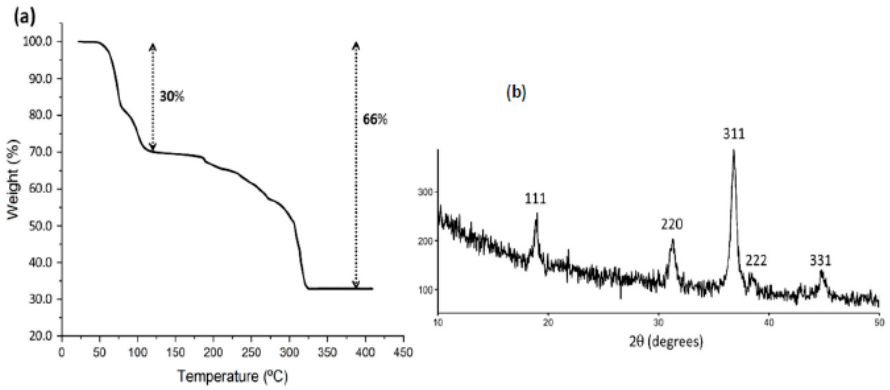

Figure 13. (**a**) TGA plot for the decomposition of a cobalt (II) acetate tetrahydrate commercial sample under air atmosphere; (**b**) XRD pattern of the final product of the ATG analysis. All the intense maxima correspond to the Co_3O_4 spinel.

Among the cobalt oxides, the most studied phase is the spinel Co_3O_4, and special attention has been paid to control its morphology. For example, J.C. Toniolo et al., [10] investigated the effect of the fuel on the microstructure of the obtained product using a combustion method. R. Itteboina et al., [7] studied the effects of precursors, solvents, and calcination temperatures on the morphology development of cobalt oxide particles with the sol–gel method. R. Samal et al. controlled crystal growth in the synthesis of Co_3O_4 nanostructures with cubic morphologies by using a hydrothermal route [35].

The morphology of the obtained Co_3O_4 was studied by SEM. Figure 15a displays a low-magnification image showing the characteristic morphology of the raw material with particle agglomeration. The high-magnification image shown in Figure 15b reveals that the nanoparticles had a rounded morphology with diameters ranging from 20 to 100 nm. These morphological characteristics are typical of solids obtained by thermal decomposition processes in which large volumes of gas are not released.

Figure 16 shows the HREM images and their corresponding FFT of two representative projections of the sample along the [001] (Figure 16a) and [110] (Figure 16b) zone axes. The lattice fringes of 0.289 nm (Figure 16a) and 0.49 nm (Figure 16b) correspond to the interplanar distances of the (020) and (111) Co_3O_4 spinel planes, respectively.

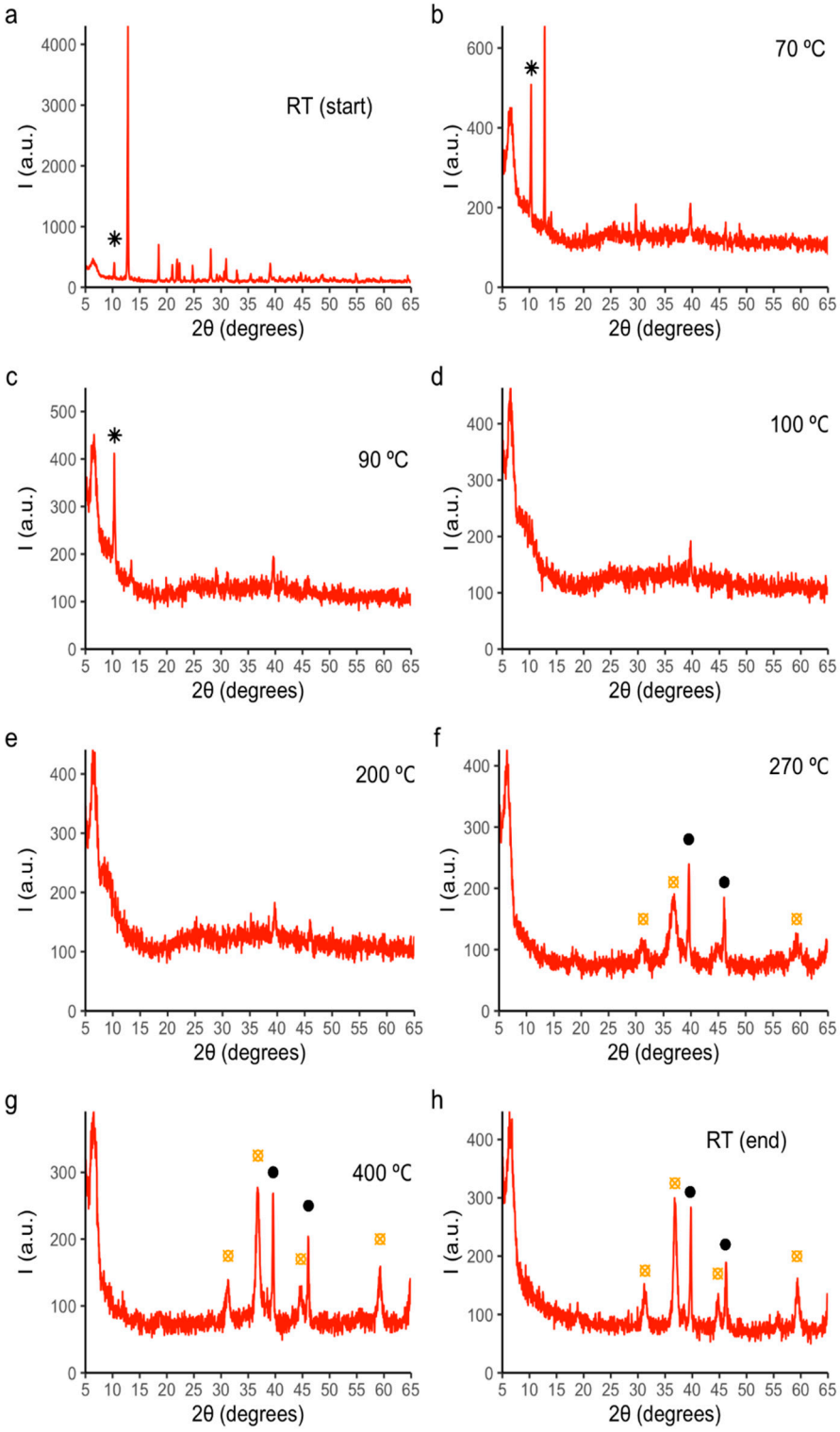

Figure 14. X-ray powder diffraction of cobalt acetate tetrahydrate heated under air atmosphere from RT to 400 °C and afterward cooled down to RT. Selected temperature steps are shown in the heating process (**a**–**g**) together with the final scan back to RT (**h**). Main phase in the starting room temperature scan is cobalt acetate tetrahydrate (PDF-00-025-0372), but the dihydrate phase (PDF-00-022-1080) can also be observed as a minor phase (main peak marked with a black asterisk in (**a**–**c**) scans). Main peaks of present phases are marked in scans (**f**–**h**) as follows: black circle for platinum (PDF-01-087-0642) and orange crossed circle for Co_3O_4 (PDF-01-086-8289).

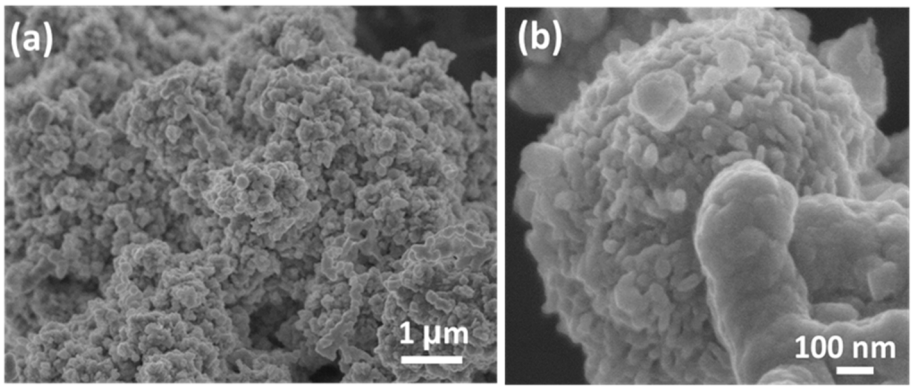

Figure 15. SEM micrographs of Co_3O_4 nanoparticles obtained at 400 °C under air: (**a**) at low-magnification (15,000×) and (**b**) at high-magnification (60,000×).

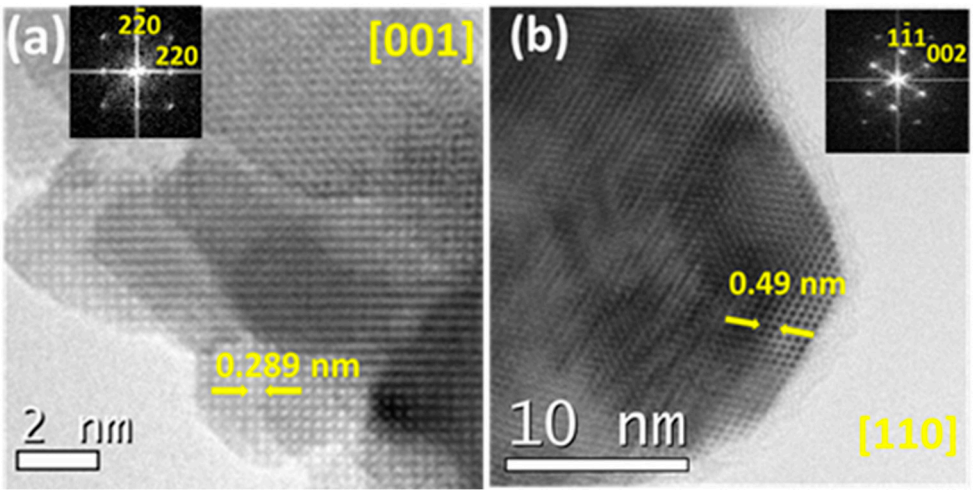

Figure 16. HRTEM images and the corresponding projections of representative nanocrystals of Co_3O_4 sample along: (**a**) [001] and (**b**) [110] projections.

4. Conclusions

This work shows how every cobalt oxide can be obtained from a single inorganic salt, cobalt (II) acetate tetrahydrate, through the careful control of the temperature and working atmosphere.

Under an N_2 atmosphere, decomposition was found to involve the loss of water at 110 °C, followed by the stabilization of a new $Co_3O(CH_3COO)_4$ intermediate phase that was isolated and whose unit cell parameters were determined with single crystal X-ray diffraction. At 330 °C, CoO with a Zn-blende structure was obtained. In fact, the Zn-blende/wurtzite ratio was found to depend not only on the temperature but also on the rate and time of heating. Subsequent heating led to rocksalt CoO as the only stable oxide at 400 °C. At this temperature, a CoO charge disproportionation process occurred to some extent, leading to both Co metal and Co_3O_4 being detected by XRD. The SEM study revealed that the morphological features of the $Co_3O(CH_3COO)_4$ precursor were retained in the final oxides, indicating a certain topotactic relationship between them. Both polymorphs comprised rounded-shape nanoparticles with an average size of 100 nm.

When the decomposition process was performed in air, the acetate abruptly broke down, resulting in the formation of Co_3O_4 at 275 °C that was maintained as the only crystalline phase observed throughout the decomposition process. This phase was composed of aggregates of round nanoparticles with diameters ranging from 20 to 100 nm.

Supplementary Materials: The following supporting information can be downloaded at https://www.mdpi.com/article/10.3390/app12136786/s1, Section I. Co (II) acetate dihydrate; Section II. X-ray diffraction pattern indexing of $Co_3O(CH_3COO)_4$. Section III. Scanning electron microscopy (SEM) study; Section IV. Thermal decomposition of $Co(CH_3COO)_2{\cdot}4H_2O$ under air.

Author Contributions: Conceptualization, methodology, validation, investigation resources, writing—original draft preparation: D.G.-M., A.V., J.M.G.-C., E.M. and M.P. E.M. carried out the X-ray diffraction measurements, and D.G.-M. carried out the electron microscopy measurements. All authors have read and agreed to the published version of the manuscript.

Funding: This research was funded by PID2020-113753RB-I00 research project.

Conflicts of Interest: The authors declare no conflict of interest.

References

1. Lin, H.-K.; Chiu, H.-C.; Tsai, H.-C.; Chien, S.-H.; Wang, C.-B. Synthesis, characterization and catalytic oxidation of carbon. *Catal. Lett.* **2003**, *88*, 169–174. [CrossRef]
2. Jansson, J.; Palmqvist, A.E.; Fridell, E.; Skoglundh, M.; Österlund, L.; Thormählen, P.; Langer, V. On the catalytic activity of Co_3O_4 in low-temperature CO oxidation. *J. Catal.* **2002**, *211*, 387–397. [CrossRef]
3. Yamaura, H.; Moriya, K.; Miura, N.; Yamazoe, N. Mechanism of sensitivity promotion in CO sensor using indium oxide and cobalt oxide. *Sens. Actuators B Chem.* **2000**, *65*, 39–41. [CrossRef]
4. Skumryev, V.; Stoyanov, S.; Zhang, Y.; Hadjipanayis, G.; Givord, D.; Nogues, J. Beating the superparamagnetic limit with exchange bias. *Nature* **2003**, *423*, 850–853. [CrossRef]
5. Roca, A.G.; Golosovsky, I.V.; Winkler, E.; López-Ortega, A.; Estrader, M.; Zysler, R.D.; Baro, M.D.; Nogués, J. Unravelling the elusive antiferromagnetic order in wurtzite and zinc blende CoO polymorph nanoparticles. *Small* **2018**, *14*. [CrossRef]
6. Sardjono, S.A.; Puspitasari, P. Synthesis and Characterization of Cobalt Oxide Nanoparticles Using Sol-Gel Method. In Proceedings of the AIP Conference Proceedings, Antalya, Turkey, 21 April 2020; Volume 2231. [CrossRef]
7. Itteboina, R.; Sau, T.K. Sol-gel synthesis and characterizations of morphology-controlled Co_3O_4 particles. *Mater. Today Proc.* **2019**, *9*, 458–467. [CrossRef]
8. Rahman, M.; Wang, J.; Deng, X.; Li, Y.; Liu, H.K. Hydrothermal synthesis of nanostructured Co_3O_4 materials under pulsed magnetic field and with an aging technique, and their electrochemical performance as anode for lithium-ion battery. *Electrochim. Acta* **2009**, *55*, 504–510. [CrossRef]
9. Xu, F.; Yan, H.; Chen, J.; Zhang, Z.; Fan, C. Nanoscale Co_3O_4 powders prepared by an enhanced solid-state reaction method. *Ceram. Int.* **2020**, *46*, 13893–13899. [CrossRef]
10. Toniolo, J.; Takimi, A.; Bergmann, C. Nanostructured cobalt oxides (Co_3O_4 and CoO) and metallic Co powders synthesized by the solution combustion method. *Mater. Res. Bull.* **2010**, *45*, 672–676. [CrossRef]
11. Vojisavljević, K.; Wicker, S.; Can, I.; Benčan, A.; Barsan, N.; Malič, B. Nanocrystalline cobalt-oxide powders by solution-combustion synthesis and their application in chemical sensors. *Adv. Powder Technol.* **2017**, *28*, 1118–1128. [CrossRef]
12. Smith, W.L.; Hobson, A.D. The structure of cobalt oxide, Co_3O_4. *Acta Crystallogr. Sect. B Struct. Crystallogr. Cryst. Chem.* **1973**, *29*, 362–363. [CrossRef]
13. Redman, M.J.; Steward, E.G. Cobaltous oxide with the zinc blende/wurtzite-type crystal structure. *Nature* **1962**, *193*, 867. [CrossRef]
14. Huang, A.F.; Banfield, J.F. Size-dependent phase transformation kinetics in nanocrystalline ZnS. *J. Am. Chem. Soc.* **2005**, *127*, 4523–4529. [CrossRef] [PubMed]
15. Grimes, R.W.; Lagerlöf, K.P.D. Polymorphs of cobalt oxide. *J. Am. Ceram. Soc.* **1991**, *74*, 270–273. [CrossRef]
16. Lou, X.W.; Deng, D.; Lee, J.Y.; Archer, L.A. Thermal formation of mesoporous single-crystal Co_3O_4 nano-needles and their lithium storage properties. *J. Mater. Chem.* **2008**, *18*, 4397–4401. [CrossRef]
17. Feng, J.; Zeng, H.C. Size-controlled growth of Co_3O_4 nanocubes. *Chem. Mater.* **2003**, *15*, 2829–2835. [CrossRef]
18. Li, C.C.; Yin, X.M.; Wang, T.H.; Zeng, H.C. Morphogenesis of highly uniform $CoCO_3$ submicrometer crystals and their conversion to mesoporous Co_3O_4 for gas-sensing applications. *Chem. Mater.* **2009**, *21*, 4984–4992. [CrossRef]
19. Zhang, H.; Wu, J.; Zhai, C.; Ma, X.; Du, N.; Tu, J.; Yang, D. From cobalt nitrate carbonate hydroxide hydrate nanowires to porous Co_3O_4 nanorods for high performance lithium-ion battery electrodes. *Nanotechnology* **2008**, *19*. [CrossRef]
20. Seo, W.S.; Shim, J.H.; Oh, S.J.; Lee, E.K.; Hur, N.H.; Park, J.T. Phase- and size-controlled synthesis of hexagonal and cubic CoO nanocrystals. *J. Am. Chem. Soc.* **2005**, *127*, 6188–6189. [CrossRef]
21. Risbud, A.S.; Snedeker, L.P.; Elcombe, M.M.; Cheetham, A.A.K.; Seshadri, R. Wurtzite CoO. *Chem. Mater.* **2005**, *17*, 834–838. [CrossRef]
22. Golosovsky, I.; Estrader, M.; López-Ortega, A.; Roca, A.; López-Conesa, L.; del Corro, E.; Estradé, S.; Peiró, F.; Puente-Orench, I.; Nogués, J. Zinc blende and wurtzite CoO polymorph nanoparticles: Rational synthesis and commensurate and incommensurate magnetic order. *Appl. Mater. Today* **2019**, *16*, 322–331. [CrossRef]

23. Dicarlo, J.; Navrotsky, A. Energetics of cobalt(II) oxide with the zinc-blende structure. *J. Am. Ceram. Soc.* **1993**, *76*, 2465–2467. [CrossRef]
24. Grimes, R.W.; Fitch, A.N. Thermal decomposition of cobalt(II) acetate tetrahydrate studied with time-resolved neutron diffraction and thermogravimetric analysis. *J. Mater. Chem.* **1991**, *1*, 461–468. [CrossRef]
25. Wanjun, T.; Donghua, C. Mechanism of thermal decomposition of cobalt acetate tetrahydrate. *Chem. Pap.* **2007**, *61*, 329–332. [CrossRef]
26. Degen, T.; Sadki, M.; Bron, E.; König, U.; Nénert, G. The HighScore suite. *Powder Diffr.* **2014**, *29*, S13–S18. [CrossRef]
27. Gates-Rector, S.; Blanton, T. The powder diffraction file: A quality materials characterization database. *Powder Diffr.* **2019**, *34*, 352–360. [CrossRef]
28. Groom, C.R.; Bruno, I.J.; Lightfoot, M.P.; Ward, S.C. The cambridge structural database. *Acta Crystallogr. Sect. B Struct. Sci. Cryst. Eng. Mater.* **2016**, *72*, 171–179. [CrossRef]
29. Kaduk, J.A.; Partenheimer, W. Chemical accuracy and precision in Rietveld analysis: The crystal structure of cobalt(II) acetate tetrahydrate. *Powder Diffr.* **1997**, *12*, 27–39. [CrossRef]
30. Sobolev, A.; Miminoshvili, E.B.; Miminoshvili, K.E.; Sakvarelidze, T.N. Cobalt diacetate tetrahydrate. *Acta Crystallogr. Sect. E Struct. Rep. Online* **2003**, *59*, m836–m837. [CrossRef]
31. Zhang, G.; Lin, J.; Guo, D.-W.; Yao, S.-Y.; Tian, Y.-Q. Infinite coordination polymers of one- and two-dimensional cobalt acetates. *Z. Anorg. Allg. Chem.* **2010**, *636*, 1401–1404. [CrossRef]
32. Jiao, X.-D.; Guzei, I.A.; Espenson, J.H. Crystal structure of catena-poly[mono(μ-aqua)di(μ-acetato)cobalt(II)] monohydrate, $[Co(CH_3COO)_2(H_2O)] \cdot H_2O$. *Z. Krist. New Cryst. Struct.* **2014**, *215*, 173–174. [CrossRef]
33. Alcalá, R.; Fernández García, J. Determinación de las estructuras cristalinas de los acetatos de hierro y cobalto. *Rev. Acad. C Exactas Fsico Químicas Nat. Zaragoza* **1973**, *28*, 303–325.
34. Doremieux, J.L. Thermal evolution of tetrahydrated cobalt acetate in a stream of nitrogen at room pressure. *Bull. Soc. Chim. Fr.* **1967**, *17*, 4593.
35. Samal, R.; Dash, B.; Sarangi, C.K.; Sanjay, K.; Subbaiah, T.; Senanayake, G.; Minakshi, M. Influence of synthesis temperature on the growth and surface morphology of Co_3O_4 nanocubes for supercapacitor applications. *Nanomaterials* **2017**, *7*, 356. [CrossRef]